RSC Advances

REVIEW

View Article Online
View Journal | View Issue

Cite this: *RSC Adv.*, 2023, **13**, 12309

An overview of the preparation and application of counter electrodes for DSSCs

Shuang Ding,[a] Chaoqiao Yang,[a] Jie Yuan, *[b] Huijin Li,[a] Xianli Yuan[a] and Min Li[b]

Received 11th February 2023
Accepted 6th April 2023

DOI: 10.1039/d3ra00926b

rsc.li/rsc-advances

Dye-sensitized solar cells (DSSCs) are potential products for the next generation of photovoltaic technology, which is one of the research hotspots in photovoltaics. The counter electrode in DSSCs collects electron in the external circuit and catalyzes the reduction of the redox electrolyte and hole transport in the solid electrolyte. Thus, it undoubtedly has an important impact on the photovoltaic performance, long-term stability, and cost of DSSCs. In this work, the materials of counter electrodes are classified into metals, carbon materials, conductive polymers, and inorganic compounds. The preparation, mechanism, conversion efficiency, and properties of counter electrodes are reviewed.

1 Introduction

Nowadays, human beings are facing increasing serious energy and climate problems. Research on renewable energy sources, such as solar energy, hydropower, geothermal energy, wind power, and tidal power, has received extensive attention. Solar energy has no geographical restrictions and can be directly collected and utilized without mining and transportation; thus, it has attracted wide research interests.

The new generation of photovoltaic technologies in solar cell research includes dye-sensitized solar cells (DSSCs), solar-driven evaporative power generation devices, perovskite solar cells (PVSCs), organic/polymer solar cells (OSCs or PSCs), and quantum dot solar cells (QDSCs). DSSCs have a simple structure and process, low production cost, easy manufacturing, and no secondary environmental pollution. Therefore, it shows high application value in solar energy development and utilization and is of great significance in research focusing on energy shortage and environmental pollution.[1–4]

2 DSSCs

DSSCs are the basis for energy conversion by injecting electrons from the photoexcited state of the dye sensitizer into the conduction band of the titanium dioxide semiconductor when absorbing light so that they may replace the traditional photovoltaic devices. They can efficiently convert solar energy into electricity with low production costs. DSSCs are composed of three main components: a dye-covered nanocrystalline titanium dioxide layer on a transparent conductive glass substrate, an iodide (I^-)/triiodide (I_3^-) redox pair in an organic solvent as an electrolyte, and a counter electrode. The counter electrode collects electrons from an external circuit and catalyzes the reduction of the redox electrolyte and the transport of holes in the solid electrolyte (Fig. 1).

Each of the components has an important role and cofunctions with each other to obtain high power conversion efficiency. The working principle of DSSCs can be summarized in the following five points.

(1) Photoexcitation of dye molecules under illumination induces charge separation.

(2) Charge (electron) is injected into the conduction band of mesoporous titanium dioxide.

(3) A charge channel is activated through an external circuit and an electronic load.

(4) The dye is reduced to the ground state by redox pairs in the electrolyte, which is usually an organic solvent containing iodide (I^-)/triiodide (I_3^-) pairs.

(5) The redox pair on the counter electrode is reduced by a charge from an external circuit, where the reaction satisfies $I_3^- + 2e^- = 3I^-$.

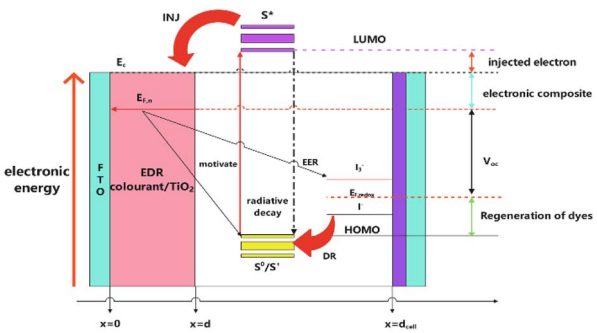

Fig. 1 Working principle of DSSCs.

[a]College of Environmental and Chemical Engineering, Dalian University, Dalian, 116622, Liaoning, China
[b]School of Chemistry and Materials Engineering, Liupanshui Normal University, Liupanshui, 553004, Guizhou, China. E-mail: yuanjieedu@163.com

The counter electrode is an extremely important part of DSSCs. Its low efficiency and instability greatly limit the photoelectric conversion efficiency and stability of solar cells.[5–8] This work mainly introduces the research progress on the preparation and application of counter electrodes.

3 Counter electrodes involving metals

Metal materials show excellent electrical conductivity, good flexibility, excellent ductility, and advanced thermal stability under high-temperature treatment. Using metal materials as the electrode substrate of solar cells can not only reduce the cost but also improve the performance of solar cells by reducing the internal resistance.

3.1 Counter electrode involving Pt

Platinum is a chemical element with the symbol Pt and an atomic number of 78. It is a dense, ductile, inert, and off-white transition metal, it is one of the least active metals, and it shows significant corrosion resistance.

The first requirement for the material used as a charge transfer agent in DSSCs is low charge transfer resistance and high exchange current density to reduce the oxidation form of the charge mediator. Due to high conductivity and catalytic activity for triiodide reduction and high reflection performance, platinum is firstly selected as the anti-electrode material for DSSCs.[9] Platinum counter electrodes can be prepared by electrochemical deposition, hot gas deposition, spray pyrolysis, cyclic voltammetry deposition, electrochemical reduction, thermal decomposition, and sputter coating.[10,11]

Cheng *et al.* sputtered a 1 nm-thick platinum film on a fluorine-doped tin oxide substrate, which was performed with thermal annealing at 400 °C. After that, the amorphous-nanocrystalline mixed platinum film became a highly crystalline one with better transmittance and electrocatalytic I_3^- reduction ability, which can be undertaken as the counter electrode of the double-sided DSSCs.[12] Yang *et al.* combined the silicon nanowires and platinum nanoparticles to prepare the counter electrode of DSSCs, which increased the photoelectric conversion efficiency to 8.32%. Firstly, it enhanced the activity of platinum by expanding the surface area. Secondly, silicon hydrogen bonds can reduce the metal ions so that small metal nanoparticles grow on the surface of silicon nanowires, thus effectively preventing the agglomeration of metal nanoparticles in catalysis.[13] Zhao *et al.* carried out a mild displacement reaction at room temperature to deposit the platinum nanoparticles on nickel foam as an efficient and flexible counter electrode.[14] Wu *et al.* successfully prepared a transparent active Pt–Mo_2C electrode for double-sided DSSCs based on the strong metal-support interaction between platinum and Mo_2C, providing the idea of building solar cells with ultrasmall size and good dispersion of platinum catalysts.[15]

3.2 Counter electrode involving non-platinum metal

The current studies prove that the performance of platinum electrode materials is undoubtedly excellent. However, platinum is a precious metal with high price, which limit its application. Therefore, good results have been reported using other metals (such as nickel, lead, rhodium, and copper) instead of platinum to prepare counter electrodes to reduce the costs.[16]

Ruthenium (Ru) is a noble metal in the platinum group, which is cheaper. It shows low resistivity, high work function, excellent thermal conductivity, and superior electrochemical stability in a wide potential range. Aftabuzzaman *et al.* prepared Ru–nitrogen doped mesoporous carbon (Ru–N-TMC) by the direct stabilization and carbonization of polybutyl acrylate-*b*-polyacrylonitrile (PBA-*b*-PAN) block copolymer and Ru acetylacetonate [$Ru(acac)_3$]. During the stabilization, microphase separation occurred in the PBAb–PAN block copolymer, and the PAN block was converted to N-doped semi-graphite carbon due to the incompatibility between the two blocks. During the carbonization, the PBA block was removed as a porous template to form layered mesopores and micropores. The obtained counter electrode shows ultralow charge transfer resistance (R_{ct} = 0.034 Ω cm^2) and high conversion efficiency of (11.16%). One of the reasons is that the nitrogen atoms can enhance the conductivity and electronic interaction between metal and carbon and improve the catalytic activity through the polarity effect.[17] More importantly, the combined effect of the small grain size of ruthenium generates many electrochemical sites, a high conductivity improves the electrocatalytic activity, and a unique network structure allows rapid electron transfer and rapid electrolyte diffusion (Fig. 2).[18,19]

In addition, iridium (Ir) has similar electrocatalytic activity due to its low resistivity. Mokurala *et al.* deposited Ir films on fluorine-doped tin oxide substrates by radio frequency sputtering to prepare the counter electrodes with a PCE of 7.2%.[20] Dao *et al.* adopted an effective and simple method to produce a gold-coated honeycomb structure substrate using a chloroform and methanol solvent immersion phase separation method with a volume ratio of 90 : 10 on a Petri dish with a high aspect ratio. A counter electrode with a high specific active area and high conductivity efficiency was obtained based on the highly-ordered cylindrical honeycomb array. The manufacturing method shows low cost, high efficiency, and good reproducibility.[21] Titanium is featured with superior stability and corrosion resistance because a natural passivation oxide is formed on

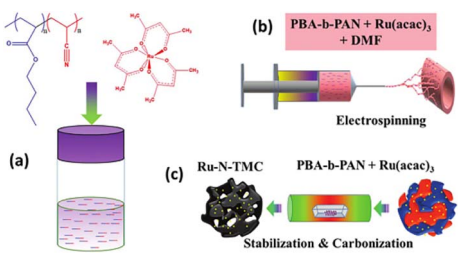

Fig. 2 Ru–N-TMC preparation; (a) homogeneous solution of PBA-*b*-PAN block copolymer and $Ru(acac)_3$ in DMF, (b) electrospinning of homogeneous solution of PBA-*b*-PAN block copolymer and $Ru(acac)_3$, (c) stabilization and carbonization of the mixture of the PBA/*b*-PAN block copolymer and $Ru(acac)_3$.

its surface. Deng *et al.* fabricated a novel $NiCo_2S_4$ nanotube counter electrode supported on a porous titanium membrane by acid etching and a two-step hydrothermal method, which can significantly improve the cell fill factor, showing excellent current density and power conversion efficiency.[22] Silver is proved to have the highest conductivity, thermal conductivity, and reflectivity among all metals and can be used as a counter electrode material for DSSCs.[23,24]

3.3 Counter electrode involving alloy

Platinum is still preferred in electrocatalysts due to its excellent electrocatalytic activity and electron conduction ability. However, the high cost is an obstacle for extensive commercial applications. Therefore, reducing the amount of platinum without sacrificing the electrocatalytic activity and stability is a lasting goal for creating promising platinum alloy electrocatalysts. Density functional theory calculations and experimental results show that platinum and transition metals (such as nickel, iron, cobalt, chromium, and palladium) platinum alloys are more active than pure platinum.[25,26] Yang *et al.* synthesized the ternary platinum alloy (Pt–M–Ni, M = Co, Pd, and Fe) counter electrodes and studied the synergistic effect on the catalytic activity. The electrocatalytic performance of ternary Pt–M–Ni alloy for I_3^- was significantly enhanced with the efficiency up to 8.71%. Li *et al.* prepared the zinc oxide nanostructure-assisted hollow platinum–nickel (PtNi) alloy microstructure counter electrode by a simple hydrothermal method and maximized the electrocatalytic behavior by adjusting the zinc precursor. The maximum power conversion efficiency of the alloyed platinum counter electrode is as high as 8.74%, which is 37.6% higher than that of the planar platinum counter electrode. In addition, the abilities to resist dissolution, charge transfer, and redox electrolytes of iodine are significantly enhanced.[27] The nickel–titanium alloy electrode prepared by Pang *et al.* had a higher charge transfer and electrocatalytic activity. The power conversion efficiency of the nickel–titanium alloy nanowire counter electrode is 8.29%.[28] Oh *et al.* successfully synthesized a series of FeSn alloy/RGO nanohybrids with different volume ratios of Fe/Sn precursors under atmospheric pressure plasma reduction and low temperature. It has a high density of surface coverage and high load of nanoparticles, which is conducive to electron transfer (Table 1).[29]

Zhao *et al.* prepared a new platinum-free Ru ternary alloy counter electrode (Ru–Co–Se) with a conversion efficiency of 9.07%, which is higher than (7.03%) that of pure platinum counter electrode.[30] The coexistence of different valence states of nickel and cobalt will generate more charge hopping and valence exchange. Wei *et al.* constructed the ternary nickel cobalt sulfide nanoparticles as the reverse electrodes of DSSCs, and their power conversion efficiency reached 8.44%.[31]

Although the pure platinum counter electrode shows excellent catalytic performance, the relatively complex preparation conditions and high cost limit its practical application. Therefore, it is a feasible way to develop platinum-based composite materials with low loading and high stability. Non-platinum metal and alloy counter electrodes have incomparable conductivity to other types of counter electrodes and have a lower cost than platinum-based counter electrodes. Therefore, further optimizing the reaction conditions, selecting relatively cheap metals, and improving their electrocatalytic activity are the focus of following research.

4 Counter electrode involving carbon material

Carbon materials are attractive candidates for counter electrode materials of DSSC to replace the traditional and expensive platinum materials due to their low cost, high specific surface area, high catalytic activity, high conductivity, high thermal stability, and good corrosion resistance to iodine. Basically, there are eight allotropes for carbon (as shown in the Fig. 3): (a) diamond, (b) graphite, (c) Randalette, (d) C_{60} (fullerene), (e) C_{540}, (f) C_{70}, (g) amorphous carbon, and (h) carbon nanotubes.[32–37]

4.1 Counter electrode involving carbon black

Carbon black (CB) nanoparticles are spherical nanosized carbon with an amorphous quasi-graphite molecular structure. Most types of CB have parallel graphite layers, and all CB surfaces have chemisorbed oxygen complexes (carboxyl, quinone, lactone, phenolic, *etc.*), which vary depending on the production conditions. CB is a good candidate material for counter electrodes due to its high electrocatalytic activity and conductivity. When CB is used for counter electrodes, its particle morphology and surface state (including size, specific surface area, porosity, crystallinity, thickness, shape, and purity) and preparation conditions are critical.[38] Kim *et al.* studied the effect of particle size and thickness of the CB porous layer on the electrochemical performance of DSSCs. CB coating

Table 1 FeSn alloy/RGO nanohybrid materials

Counter electrode	ΔE (mV)	R_{trns} (Ω)	R_{ct} (Ω)	Z_w (Ω)	J_{sc} (mA cm^2)	V_{oc} (mV)	FF (%)	PCE (%)
Fe_0Sn_1/RGO	400	2.04	0.38	36.21	10.50	660	66.52	4.6
$Fe_{0.1}Sn_{0.9}$/RGO	330	1.66	0.36	28.55	11.32	660	66.38	5.0
$Fe_{0.3}Sn_{0.5}$/RGO	450	2.07	0.43	31.10	9.80	655	67.92	4.4
$Fe_{0.5}Sn_{0.5}$/RGO	435	2.08	0.47	32.23	9.40	650	68.69	4.2
$Fe_{0.7}Sn_{0.3}$/RGO	450	3.19	0.50	31.94	9.17	635	69.32	4.0
$Fe_{0.9}Sn_{0.1}$/RGO	440	3.20	0.51	31.36	8.85	660	68.77	4.0
Fe_1Sn_0/RGO	470	5.15	0.56	34.71	8.50	645	68.31	3.8

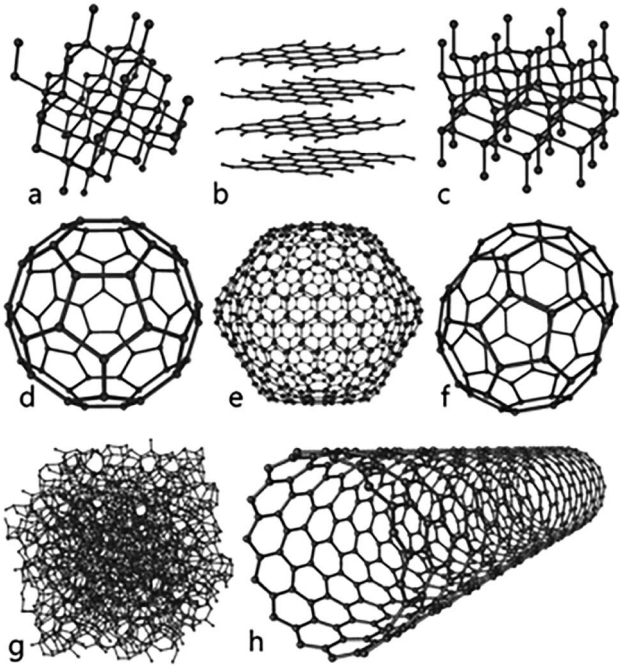

Fig. 3 Allotropes of carbon.

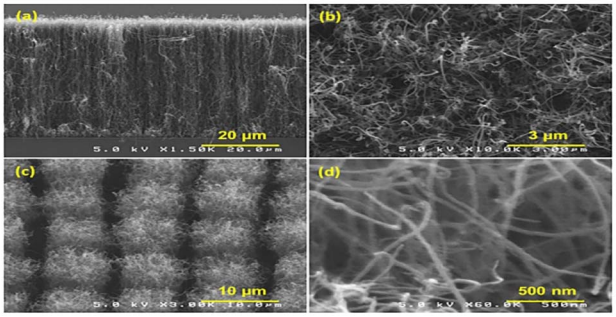

Fig. 4 (a) and (b) Cross-sectional and top-view SEM micrographs of P-CNTs (planar CNTs) grown on a silicon substrate with a height of ~45 μm and the porous structure of the CNT network; (c) and (d) tilted-view SEM micrographs of MA-CNTs (micro-array patterned CNTs) at 3k and 60k magnifications, showing a part of the array of CNTs and the CNT tube diameter of ~30–50 nm.

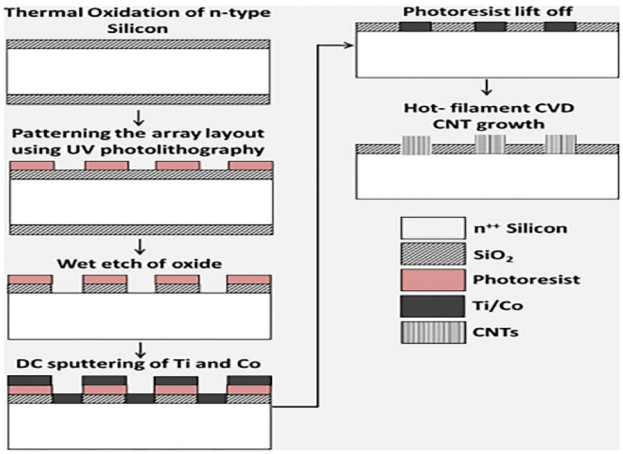

Fig. 5 Fabrication process for the micro-array patterned CNT (MA-CNT) electrodes.

was sprayed on fluorine-doped tin oxide (FTO) glass at 120 °C. The size of CB particles varies from 20 to 90 nm. By controlling the spraying time, the thickness of the CB counter electrode is controlled at 1–9 mm. With the decrease in the CB particle size, the specific surface area and conductivity of the CB layer increase, and so does the catalytic activity. The increase in the thickness of the CB counter electrode can also improve the catalytic activity, but the charge transfer resistance at the electrolyte/CB counter electrode interface will increase. The photoelectric conversion efficiency of the CB counter electrode is 7.2% when the particle size is 20 nm and the thickness is 9 mm.[39] CB nanoparticles are relatively cheaper than other nanostructures and show excellent catalytic ability. However, they are reportedly carcinogenic and can cause health problems.

4.2 Counter electrode involving carbon nanotubes

Carbon nanotubes are allotropes of carbon with cylindrical nanostructures. Its walls are made of single-atom-thick carbon sheets (*i.e.*, graphene). The carbon nanotubes may contain one or more concentric shells of graphene sheets, called single-walled carbon nanotubes (SWCNT) or multiwalled carbon nanotubes (MWCNT). In addition, it may have open or closed ends. Carbon nanotubes have extraordinary strength, hardness, electrical conductivity, thermal conductivity, and mechanical strength. Zheng *et al.* applied a simple, fast, and cost-effective strategy to grow the MWCNT nanocomposites *in situ* on nickel substrates by the ethanol flame method and verified that the photoelectric conversion efficiency can reach up to 7.43%.[40] Yilmaz *et al.* employed the hot filament chemical vapor deposition to directly grow the carbon nanotubes with planar and microarray structures on highly doped N-type silicon substrates without using any additives and binders. The N-719 dye-sensitized titanium dioxide was coated on a fluorine-doped tin dioxide glass substrate as a photoanode and an iodine-based electrolyte. The carbon nanotubes with a planar structure as a counter electrode showed a very high photocurrent density of 26.3 mA cm^{-2} and a power conversion efficiency of 7.13%.[41] Yue *et al.* synthesized a ternary composite $MoIn_2S_4$@-CNTs counter electrode with a hedgehog ball structure by a simple one-step hydrothermal method. The analysis showed that it has a larger specific surface area, is conducive to the adsorption of more electrolyte, provides a greater active contact area for the electrode, and increases the power conversion efficiency to 8.38% (Fig. 4 and 5).[42]

4.3 Counter electrode involving carbon nanofibers

Carbon nanofibers have a large surface volume ratio, adjustable transmission characteristics, and unique surface chemical properties. They can also be used as counter electrodes. Wang *et al.* used nanocopper particles as catalysts to prepare the helical carbon nanofibers instead of platinum for counter

electrodes by acetylene pyrolysis. They were proved to have high surface area and excellent catalytic performance, and the energy conversion efficiency of the solar cells was 6.74%.[43] Li *et al.* prepared the nitrogen-doped cobalt-based carbon nanofibers by electrospinning to prepare counter electrodes, which showed a high power conversion efficiency of 9.05% at an illumination of 100 mW cm^{-2}.[44] Compared with carbon nanotubes and carbon nanoparticles, the size of the carbon nanofibers is larger, which limits the effective surface areal thus, a thicker carbon nanofiber layer is required to reduce the overall resistance.[45,46]

4.4 Counter electrode involving graphene

Graphene is a new type of nanomaterial, which is composed of a single carbon atom arranged in a hexagonal lattice. Its properties are excellent, supported by high surface area (2630 m^2 g^{-1}), high thermal conductivity (5000 W mK^{-1}), fast charged carrier mobility (200 000 cm^2 V^{-1} s^{-1}), high transmittance (97.7%), and high chemical inertness.[47–49] Wu *et al.* studied the preparation of graphene nanosheet (GNF) membrane on FTO glass by the scraper method and thermal annealing at different temperatures in air and argon atmosphere. The GNF/FTO membrane was undertaken as the counter electrode of DSSCs. It was found that the GNF/FTO membrane can more effectively improve the PCE value of DSSC when annealed in an argon atmosphere with a temperature higher than 380 °C.[50] Yu *et al.* developed a three-dimensional (3D) graphene/SWCNT counter electrode for DSSCs by the drop coating method and proved that the power conversion efficiency was excellent (9.24%), and it can be increased to 10.56% when the mirror is set below the battery.[51] Tang *et al.* utilized the reduced graphene oxide (RGO) to fully contact with the electrolyte and 3D graphene networks (3DGNs) to provide a fast electron transport channel so that the I_3^-/I^- redox reaction is accelerated to the greatest extent; thus, the power conversion efficiency is as high as 9.79%.[52] Chen *et al.* adopted CO_2 and sodium to generate the 3D graphene as the counter electrode of DSSC, which is an environment friendly, low-cost, simple, and commercially available method for preparing counter electrodes, and most importantly, can help control the emission of carbon dioxide.[53]

4.5 Counter electrode involving mesoporous carbon

As a new type of nanocarbon material, mesoporous carbon material has attracted wide attention due to its high specific surface area, high conductivity, large pore size, and high chemical stability. These structural characteristics endow it with potential application prospects in catalysis, adsorption, and energy storage.[54,55] Younas *et al.* synthesized highly mesoporous carbon with different porous structure characteristics (mesoporous size, pore volume, and specific surface area) and evaluated it as an electrocatalyst on the counter electrode of DSSC. The photovoltaic efficiency of DSSC is positively correlated with the pore size and pore volume. The high photovoltaic efficiency is attributed to the increased electrocatalytic activity observed in the Tafel study and is due to the increased recombination resistance and decreased electron transfer resistance found in the EIS study. In an electrolytic environment, mesoporous carbons have higher photovoltaic efficiency and stability than the platinum counterparts.[56] Wang *et al.* coated the mesoporous carbon slurry on FTO glass substrate to prepare a novel carbon counter electrode for DSSCs. Mesoporous carbon with a pore size of 6.8 nm was uniformly distributed on the conductive substrate. The electrocatalytic activity of mesoporous carbon electrode for triiodide reduction was studied by electrochemical impedance spectroscopy. The filling coefficient was 65% and the photoelectric conversion efficiency was 6.18%.[57]

Due to the low cost, chemical inertness, and particularly high catalytic activity, various forms of carbon materials are promising alternatives to traditional platinum. In addition, carbon compounds play a vital role in regulating the photoelectric properties by adjusting the short-circuit current, open-circuit voltage, and fill factor. Therefore, further research on the correlation between its catalytic activity and its physical and chemical properties is still in progress to construct a high-performance carbon counter electrode and accelerate its practical application.

5 Counter electrode involving conductive polymers

Conducting polymers are derivatives of polyacetylene, polyaniline (PANI), polypyrrole (PPy), or polythiophene. The molecular structure of these polymers is characterized by conductive conjugated double bonds. Due to its easy synthesis, high conductivity, low cost, abundance, and good catalytic performance, conductive polymers not only show unique light absorption properties but also can be used as hole transport materials; thus, it can be a counter electrode material of DSSCs. The following are typical conductive polymers and their structures and the electrical conductivity of some conductive polymers (Fig. 6 and Table 2).[58,59]

5.1 Counter electrode involving PPy

In recent years, PPy has attracted increasingly more attention as a potential candidate material for platinum counter electrodes due to its high stability, good electrochemical performance, and easy preparation. By placing FTO/glass substrate on the PPy of methyl orange-ferric chloride complex, Jha *et al. in situ* prepared PPy needle-like nanorod membranes, which shows the catalytic activity for the I_3^-/I^- redox pairs.[60] Wang *et al.* prepared the hierarchical PPy (HNPPy) with spherical PPy nanoparticles on the surface of PPy nanofiber network by a simple process. This unique hierarchical nanostructure can simultaneously provide fast electron transfer pathways and abundant electrocatalytic active sites, and its conversion efficiency reaches 6.78%.[61] Hou *et al.* electropolymerized PPy on a FTO substrate coated with MWCNTs to obtain a composite conductive polymer, in which MWCNTs are encapsulated by 15 nm-thick PPy nanoparticles. Utilizing the high surface area and good conductivity of MWCNTs and the good catalytic activity of PPy for the reduction of triiodide to iodide, it provides fast electron transport and

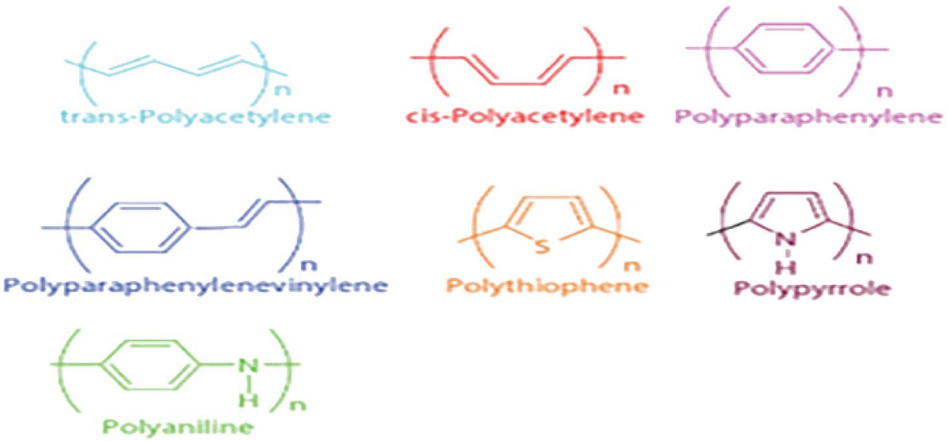

Fig. 6 Typical conductive polymers and their structures.

Table 2 Conductivities of some conductive polymers

Polymer	Conductivity (S cm^{-1})
(1) Polyacetylene	10^3 to 1.7×10^5
(2) Poly(3,4-ethylene-dioxythiophene)	10^3
(3) Polypyrrole	10^2 to 7.5×10^3
(4) Polythiophene	10 to 10^3
(5) Poly(*p*-phenylene-vinylene)	3 to 5×10^3
(6) Poly-*para*-vinylene	1–10^3
(7) Poly-*para*-phenylene sulfide (PPS)	3–300
(8) Polyaniline	30–200
(9) Polyisothionaphthene	1–50

diffusion channels and a large number of interfacial catalytic active sites, and the photoelectric conversion efficiency is 7.15% (Fig. 7).[62]

Li *et al.* introduced a low-cost, translucent, and honeycomb PPy/MWCNT capillary electrophoresis double-sided DSSC. The photoelectric conversion efficiency was 7.07%, which was not high, but this simple template method can be widely applied to prepare other cost-effective and transparent double-sided solar cells and tandem devices.[63]

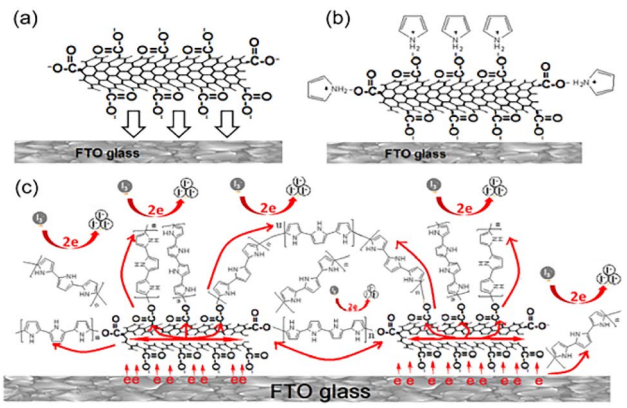

Fig. 7 A schematic diagram of the catalytic mechanism of PPy/carbon nanotubes: (a) preparation of MWCNTs on MWCNTs substrate, (b) adsorption of pyrrole monomer on MWCNTs surface, (c) electrochemical polymerization of PPy on MWCNTs and MWCNTs substrate.

5.2 Counter electrode involving PANI

PANI can be used to manufacture conductive yarns, antistatic coatings, and flexible electrodes because of its low cost, easy synthesis, high conductivity, high thermal stability, and good redox properties.[64,65] It is very difficult to deposit PANI membrane on the surface of FTO glass. Shahid *et al.* reported a new method for depositing PANI on porous single-layer graphene carrier by *in situ* polymerization. First, the graphene slurry was coated on a bare FTO glass and sintered. Then, the graphene-coated FTO glass was immersed in acidified aniline and ammonium persulfate solutions. The dissolved aniline molecules flow through the porous graphene membrane. After cooling in the ice bath, the PANI nanofibers begin to grow in the porous graphene framework. Therefore, due to the sudden growth expansion, the PANI nanofibers are closely wedged with the graphene surface. This graphene-loaded PANI hybrid structure (Gr/PANI) counter electrode shows a light conversion efficiency of 3.58%, which is 90% that of platinum-based DSSCs (Fig. 8).[66]

Polyvinyl pyrrolidone/PANI nanocomposites were synthesized by Gao *et al.* and undertaken as transparent counter electrodes for double-sided quasi-solid-state DSSCs. Aniline-coated polyvinyl pyrrolidone can effectively stabilize the space in the polymerization. The presence of polyvinyl pyrrolidone in PANI capillary electrophoresis promoted the formation of active reaction sites at the interface between the counter electrode and the electrolyte, further reducing the electron recombination. The power conversion efficiency of the DSSCs prepared by polyvinyl pyrrolidone (4%)/PANI capillary electrophoresis was 5.45%, which was comparable to that of DSSCs assembled by platinum capillary electrophoresis.[67] Zatirostami *et al.* used PANI, tungsten trioxide (WO_3) and their composites deposited on indium oxide membrane substrates by cyclic voltammetry to prepare the counter electrodes with an efficiency of 6.78%, which was 12.4% higher than that of platinum-based DSSCs.[68]

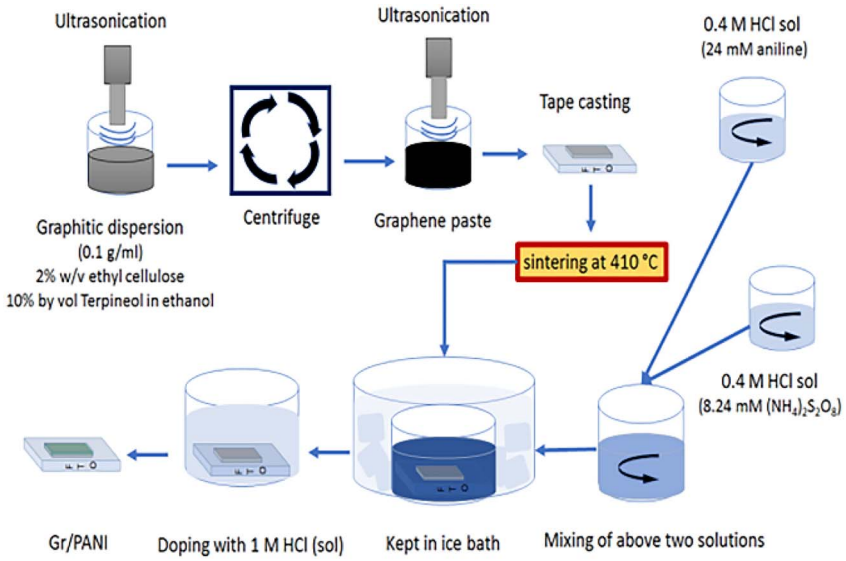

Fig. 8 Experimental procedure description of graphene-supported hybrid PANI counter electrode (Gr/PANI) and DSSC preparation.

5.3 Counter electrode involving poly(3,4-ethylenedioxythiophene) (PEDOT)

PEDOT has been widely studied as an efficient catalyst for DSSCs due to its nanoporous structure, high room temperature conductivity, high electrochemical reversibility, and significant chemical and thermal stability.[69] With conductive polymer PEDOT, polystyrene sulfonate (PSS) (PEDOT:PSS), and insulating halloysite nanotubes (HNTs) as fillers, water-based viscous screen printing ink was prepared by Gemeiner *et al.* through a simple homogenization process. PSS/HNTs inks were screen-printed on FTO substrates and used as counter electrodes for DSSCs.[70] Ma *et al.* prepared flexible PEDOT counter electrodes on doped indium tin oxide (ITO)-coated polyethylene naphthalene (PEN) (ITO-PEN) substrate by the electrochemical method for DSSCs. The effect of deposition time on the catalytic activity of flexible PEDOT electrodes for iodide redox couple was also studied. After optimization, the power conversion efficiency of DSSCs deposited with the PEDOT counter electrode for 80 seconds was 7.18%, which was close to that of DSSCs with the platinum counter electrode. The platinum/PDEOT composite catalyst was synthesized to further improve the catalytic activity of PEDOT, and its PCE was 7.90%.[71] Xiao *et al.* used pulsed potentiostatic electropolymerization to electropolymerize the high-performance nanomeadow poly-PEDOT onto FTO substrates as counter electrodes for DSSCs and studied various pulse parameters to control the morphology of PEDOT membranes. It was found that the photoelectric energy conversion efficiency applied to the counter electrode is 6.40% under 1.2 V pulse conduction potential, 0.2 V pulse reversal potential, 1 s pulse conduction period, 0.5 s pulse reversal period, and a total of 900 durations.[72]

The conductive polymers show low cost and simple preparation process but low catalytic activity and conductivity. Finding a suitable method to prepare the conductive polymer counter electrodes with controllable morphology and large specific surface area is an important direction for future research.

6 Counter electrode involving inorganic compound

In recent studies, inorganic compounds have shown electrocatalytic activity in the reduction of triiodide and have been used as catalytic materials in DSSCs. Compared with carbon materials and organic polymers, inorganic compounds exhibit unique properties such as a wide variety of materials, good plasticity, and simple manufacturing.[73–75]

6.1 Counter electrode involving carbon compound

The potential applications of carbon compounds in material chemistry have been widely explored due to their high electrical and thermal conductivity, good chemical stability, excellent catalytic activity, and low-temperature superconductivity. Ko *et al.* studied the heating layered tungsten oxide at 700 °C, 800 °C, and 900 °C to prepare the tungsten carbide particles as counter electrodes for DSSCs. The sample heated at 800 °C showed a dominant tungsten carbide structure and a relatively high specific surface area. The improvement in the photoelectrochemical properties of the samples prepared at 800 °C may be due to the catalytic activity of the tungsten carbide phase and the highly active sites for iodide reduction.[76] Guo *et al.* greatly improved the catalytic activity of carbides by embedding carbide particles into carbon carriers to prepare the composite counter electrodes. Some carbon-supported carbides even performed better than platinum. High power conversion efficiencies of 9.75, 9.42, and 9.19% were achieved using VC–C, WC–C, and Mo_2C–C, respectively, which are much higher than that of platinum counter electrode (8.18%).[76] This is conducive to improving the catalytic activity by synthesizing the composite catalysts and making the industrialization of direct reduction of

Table 3 Performance comparison of carbides

CE catalysts	V_{oc}/mV	J_{sc}/mA cm^{-2}	FF	PCE/%	R_s/Ω cm^2	R_{ct}/Ω cm^2	Z_N/Ω cm^2
Cr_2C_3	834	12.10	0.535	5.40	32.34	10.75	22.92
Cr_2C_3–C	841	14.47	0.686	8.36	31.65	1.40	16.49
Mo_2C	823	12.94	0.624	6.64	31.19	5.32	26.99
Mo_2C–C	838	15.38	0.713	9.19	31.54	0.80	13.46
WC	839	13.16	0.651	7.19	31.28	4.11	23.68
WC–C	842	15.52	0.721	9.42	30.73	0.59	10.54
VC	837	13.21	0.663	7.33	31.31	3.68	12.06
VC–C	840	15.86	0.732	9.75	30.99	0.48	5.78
NbC	836	12.27	0.61	6.26	31.80	6.13	23.75
NbC–C	842	13.78	0.679	7.89	31.25	2.56	7.42
TaC	833	13.29	0.674	7.45	31.75	3.46	14.94
TaC–C	835	14.59	0.703	8.56	31.23	1.32	7.83
TiC	831	13.00	0.652	7.05	31.12	4.25	29.93
TiC–C	847	14.91	0.701	8.85	32.14	1.26	10.56
ZrC	825	12.08	0.494	4.93	32.23	11.1	38.55
ZrC–C	837	13.75	0.665	7.66	32.48	3.02	17.27
HfC	835	12.43	0.55	5.71	32.77	9.01	17.77
HfC–C	846	13.60	0.678	7.81	32.25	2.80	13.43
Pt	836	14.16	0.691	8.18	31.30	1.82	11.13

carbon possible using carbon-supported transition metal carbide catalysts (Table 3).

Kim *et al.* prepared the nanostructured iron carbide/carbon composites by electrochemically anodizing iron foil and then heated it in a carbon-containing gas atmosphere, forming a conformal carbon shell on the surface of crystalline Fe_3C. Based on various electrochemical characterization methods, it was confirmed that the catalytic performance of iron carbide/carbon composites in cobalt bipyridine redox electrolyte was better than that of platinum. When used as an anti-electrode in DSSCs, the composite showed superior performance in increasing the power conversion efficiency by 8.0% compared to platinum anti-electrodes (Fig. 9).[77]

6.2 Counter electrode involving chalcogenide

Chalcogenides include sulfides, selenides, and tellurides. Metal chalcogenides have different compositions, molecular structures, unique properties, and excellent catalytic activity for I_3^-; thus, they can be adopted as counter electrodes. After Yu *et al.* sprayed the metal chalcogenide $N_4H_9Cu_7S_4$ solution, the Cu_2S membrane was obtained on the FTO glass substrate by sintering to prepare a counter electrode. Compared with the platinum counter electrode, the Cu_2S counter electrode showed higher electrocatalytic activity and lower charge transfer resistance; thus, its photoelectric efficiency was higher.[78] Subbiah *et al.* successfully synthesized the silica and molybdenum disulfide-coated silica nanocomposites by a hydrothermal method to

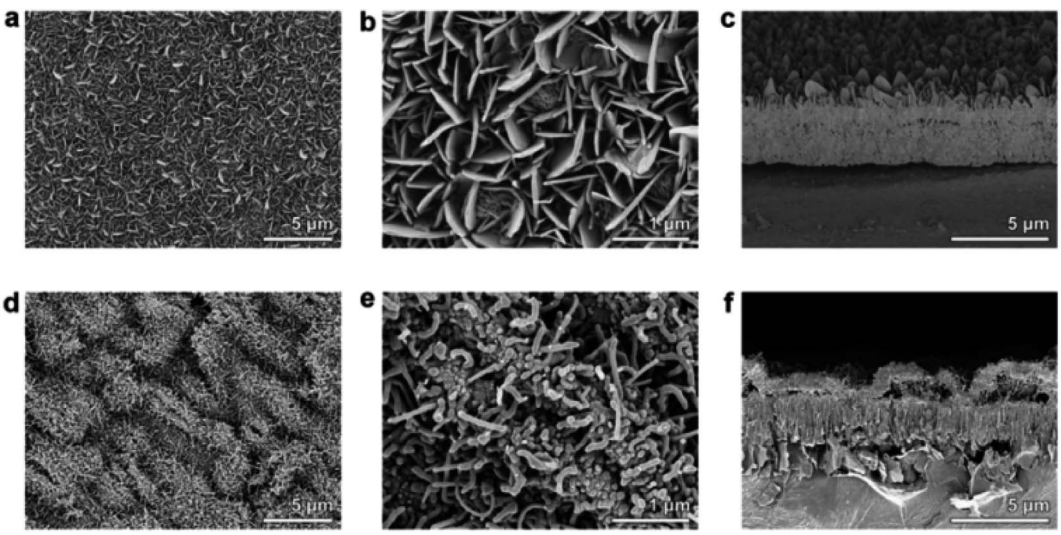

Fig. 9 (a) SEM image of FeO_x, (b) SEM image of Fe_3C/C, (c) top view of FeO_x cross section, (d) and (e) top view of Fe_3C/C, and (f) Fe_3C/C cross-section.

prepare the counter electrodes for DSSCs. In particular, the oxidation state of the molybdenum atom can exist in the range of +2–+6 so that the molybdenum atom can easily participate in the redox reaction, thus greatly improving the photoelectric conversion efficiency.[79] The ultrathin nanostructures of metal chalcogenides exhibit excellent electrocatalytic activity due to the high percentage of surface atoms and many exposed internal atoms, which inevitably induced the formation of defects as efficient active sites. Zhang *et al.* firstly reported a high-performance electrocatalyst of ultrathin Ni–Ni_3Se_2 nanosheets on graphene nanosheets. The specific surface area of the ultrathin Ni–Ni_3Se_2/graphene nanoflakes was as high as 162.5 $m^2\ g^{-1}$ when the thickness of the obtained nanoflakes was 1.5–2.5 nm. The electrocatalytic activity of nickel–nickel oxide/graphene nanosheets was measured as the counter electrode of DSSCs. Ni–Ni_3Se_2/graphene nanosheets had high iodine reduction performance, and the power conversion efficiency was 7.76%, which was higher than that of platinum-based reference electrodes (7.42%).[80]

6.3 Counter electrode involving nitrogen compound

The electronic structure of transition metal nitrides is similar to that of noble metals. Some transition metal nitrides exhibit platinum-like electrocatalytic activity. Vanadium nitride (VN) is a low-cost inorganic material due to its high conductivity and electrochemical activity. Wang *et al.* prepared the 3D porous VN nanobelt aerogels by annealing in ammonia or argon atmosphere after a simple hydrothermal process and used them as counter electrodes for DSSCs. Its high porosity and fewer grain boundaries are conducive to electron transport and electrolyte diffusion; thus, a large accessible surface area is beneficial to increase the electrolyte/electrode contact area and the number of electrocatalytic active sites. This counter electrode achieved a conversion efficiency of 7.05% by differential scanning calorimetry, which was very close to the that of batteries with conventional platinum counter electrodes.[81] CB-silicon nitride (CB–Si_3N_4) nanocomposites were applied by Ahmed *et al.* as cost-effective counter electrodes for DSSCs. CB-Si_3N_4 nanocomposites were coated on FTO substrates by screen printing. The results showed that when the thickness was 4.7 μm; the CB-Si_3N_4 composite counter electrode exhibited lower charge transfer resistance and higher electrocatalytic activity for the reduction of triiodide on CB and Si_3N_4 electrodes.[82]

6.4 Counter electrode involving oxygen compound

Oxygen compounds are different from carbon compounds, nitrogen compounds, and chalcogenides. Transition metal oxides are rarely used as the counter electrode to replace WO_2 nanorods synthesized by platinum Wu *et al.* DSSCs with WO_2 counter electrode showed a photoelectric conversion efficiency of 7.25% and good catalytic activity.[83] A cubic crystal nickel oxide membrane was synthesized by Yadav *et al.* using a chemical bath deposition method, which exhibited a porous honeycomb morphology and was more efficient than the counter electrode prepared by pure platinum.[84] Tsai *et al.* prepared CuO and CuO/graphene slurry and coated it on FTO glass substrate by a scraper coating method. The substrate was then sintered at 350 °C to form CuO and CuO/graphene nanostructures with conversion efficiencies of 2.73% and 3.40%, respectively. It showed a simple manufacturing process and low price.[85]

Inorganic compound counter electrodes not only show high catalytic activity but also have considerable stability, showing great application prospects and potential. Due to the wide variety, inorganic compounds that have been prepared and applied to DSSC counter electrode materials are only a small part of this large family; thus, there is still a broad space for research and exploration.

7 Prospects and future

DSSC is one of the typical representatives of third-generation solar cells, which is advanced with low cost, simple preparation, excellent efficiency, and high environmental friendliness. The counter electrode is a key component, which affects the photovoltaic performance and device cost of solar cells greatly. A counter electrode must have high conductivity, good electrolyte regeneration catalytic activity, and superior stability. Platinum can meet all the requirements of counter electrodes and is the most used counter electrode material. However, high cost and insufficient stability limit its wide application. Low cost, simple preparation, and good stability make carbon materials a stronger competitor. However, its conductivity and catalytic activity are relatively low; the dose required to obtain the target catalytic activity is large, and the adhesion to the substrate is poor. Conductive polymers are flexible, transparent, easy to process, and easy to adjust. Among the conductive polymers, PEDOT shows the best performance but high cost. PPy is cheaper but the performance is not as good as PEDOT. Inorganic compounds have high stability and good catalytic activity; thus, single-phase metal oxides and sulfides can be used as counter electrode materials. However, its efficiency, electrochemical cycle stability, and catalytic performance are not good compared with platinum. Different materials exhibit various and unique disadvantages and advantages; thus, it is an important direction to prepare two or more materials into composite materials by physical or chemical methods to integrate the properties of various materials.

Conflicts of interest

The authors declare that there is no conflict of interest regarding the publication of this paper.

Acknowledgements

This work was supported by the Chinese National Natural Science Foundation (51904150), Basic Research Program of Guizhou Province ([2020]1Y225), Guizhou Province Ordinary Universities Scientific Talents Project (KY[2019]056). Liupanshui Science and Technology Plan Project (No. 52020-2022-PT-04).

References

1 M. Grätzel, *J. Photochem. Photobiol., A*, 2004, **164**, 3–14.
2 Md. K. Nazeeruddin, R. Humphry-Baker, P. Liska and M. Grätzel, *J. Phys. Chem. B*, 2003, **107**, 8981–8987.
3 H.-J. Ahn, J.-S. Lee, H.-S. Kim, I.-T. Hwang, J.-H. Hong, J. Shin and C.-H. Jung, *J. Ind. Eng. Chem.*, 2018, **65**, 318–324.
4 X. D. Yang, D. B. Liu, Y. Hu, G. Wang, G. D. Zhou, P. Li, B. Wu and Q. L. Song, *Chem. Phys.*, 2018, **513**, 73–77.
5 S.-S. Kim, Y.-C. Nah, Y.-Y. Noh, J. Jo and D.-Y. Kim, *Electrochim. Acta*, 2006, **51**, 3814–3819.
6 A. Capasso, S. Bellani, A. L. Palma, L. Najafi, A. E. Del Rio Castillo, N. Curreli, L. Cinà, V. Miseikis, C. Coletti, G. Calogero, V. Pellegrini, A. Di Carlo and F. Bonaccorso, *2D Mater.*, 2019, **6**, 035007.
7 A. Rani, K. Chung, J. Kwon, S. J. Kim, Y. H. Jang, Y. J. Jang, L. N. Quan, M. Yoon, J. H. Park and D. H. Kim, *ACS Appl. Mater. Interfaces*, 2016, **8**, 11488–11498.
8 R. Irani, N. Naseri and S. Beke, *Coord. Chem. Rev.*, 2016, **324**, 54–81.
9 K.-M. Lee, L.-C. Lin, C.-Y. Chen, V. Suryanarayanan and C.-G. Wu, *Electrochim. Acta*, 2014, **135**, 578–584.
10 J. S. Dondapati, A. R. Thiruppathi, A. Salverda and A. Chen, *Electrochem. Commun.*, 2021, **124**, 106946.
11 M. Özkan, S. G. Hashmi, J. Halme, A. Karakoç, T. Sarikka, J. Paltakari and P. D. Lund, *Org. Electron.*, 2017, **44**, 159–167.
12 C.-E. Cheng, Z.-K. Lin, Y.-C. Lin, B.-C. Lei, C.-S. Chang and F. S.-S. Chien, *Jpn. J. Appl. Phys.*, 2017, **56**, 012301.
13 L. Yang, Y. Ji, F. Liao, Y. Cheng, Y. Sun, Y. Li and M. Shao, *Electrochim. Acta*, 2018, **271**, 261–267.
14 A. Zhao, S. Huang, J. Huang, P. Hu, H. Mao, C. Chen, Y. Li and M. Wei, *Sol. Energy*, 2021, **224**, 82–87.
15 C. Wu, R. Li, Y. Wang, S. Lu, J. Lin, Y. Liu and X. Zhang, *Chem. Commun.*, 2020, **56**, 10046–10049.
16 S. Yun, A. Hagfeldt and T. Ma, *Adv. Mater.*, 2014, **26**, 6210–6237.
17 M. Aftabuzzaman, C. K. Kim, H. Zhou and H. K. Kim, *Nanoscale*, 2020, **12**, 1602–1616.
18 G.-H. An, B.-R. Koo and H.-J. Ahn, *Phys. Chem. Chem. Phys.*, 2016, **18**, 6587–6594.
19 G.-H. An, J. I. Sohn and H.-J. Ahn, *J. Mater. Chem. A*, 2016, **4**, 2049–2054.
20 K. Mokurala, A. Kamble, P. Bhargava and S. Mallick, *J. Electron. Mater.*, 2015, **44**, 4400–4404.
21 V.-D. Dao, V.-T. Bui, M. Baek, T.-L. Phan, K. Yong and H.-S. Choi, *Chem. - Eur. J.*, 2018, **24**, 561–566.
22 J. Deng, M. Wang, X. Song, Z. Yang and Z. Yuan, *Nanomaterials*, 2018, **8**, 251.
23 J. Xia, C. Yuan and S. Yanagida, *ACS Appl. Mater. Interfaces*, 2010, **2**, 2136–2139.
24 K. Susmitha, M. Naresh Kumar, L. Giribabu, S. Narendra Babu and M. Raghavender, *J. Mater. Sci.: Mater. Electron.*, 2016, **27**, 5802–5809.
25 J. Greeley, I. E. L. Stephens, A. S. Bondarenko, T. P. Johansson, H. A. Hansen, T. F. Jaramillo, J. Rossmeisl, I. Chorkendorff and J. K. Nørskov, *Nat. Chem.*, 2009, **1**, 552–556.
26 M. Li, Y. Lei, N. Sheng and T. Ohtsuka, *J. Power Sources*, 2015, **294**, 420–429.
27 P. Li, Y. Zhang, W. Fa, X. Yang and L. Wang, *J. Power Sources*, 2017, **360**, 232–242.
28 Z. Pang, Y. Zhao, Y. Duan, J. Duan, Q. Tang and L. Yu, *J. Energy Chem.*, 2019, **30**, 49–56.
29 H.-J. Oh, V.-D. Dao, K.-H. Ryu, J.-H. Lee and H.-S. Choi, *J. Alloys Compd.*, 2018, **754**, 139–146.
30 Y. Zhao, J. Duan, Y. Duan, H. Yuan and Q. Tang, *Mater. Lett.*, 2018, **218**, 76–79.
31 P. Wei, J. Li, H. Kang, Z. Hao, Y. Yang, D. Guo and L. Liu, *Sol. Energy*, 2019, **188**, 603–608.
32 H. Choi, H. Kim, S. Hwang, W. Choi and M. Jeon, *Sol. Energy Mater. Sol. Cells*, 2011, **95**, 323–325.
33 G. Veerappan, K. Bojan and S.-W. Rhee, *ACS Appl. Mater. Interfaces*, 2011, **3**, 857–862.
34 S. S. Nemala, K. S. Aneja, P. Bhargava, H. L. M. Bohm, S. Mallick and S. Bohm, *Electrochim. Acta*, 2018, **285**, 86–93.
35 Z. Chen, F. Lei and C. Yuan-Fu, *Acta Phys. Sin.*, 2019, **68**, 017802.
36 I.-P. Liu, Y.-C. Hou, C.-W. Li and Y.-L. Lee, *J. Mater. Chem. A*, 2017, **5**, 240–249.
37 U. Mehmood, A. Ur Rehman, H. M. Irshad, A. Ul Haq Khan and A. Al-Ahmed, *Org. Electron.*, 2016, **35**, 128–135.
38 A. Kay and M. Grätzel, *Sol. Energy Mater. Sol. Cells*, 1996, **44**, 99–117.
39 J.-M. Kim and S.-W. Rhee, *Electrochim. Acta*, 2012, **83**, 264–270.
40 L. Zheng, C. Bao, S. Lei, J. Wang, F. Li, P. Sun, N. Huang, L. Fang and X. Sun, *Carbon*, 2018, **133**, 423–434.
41 M. Yilmaz, S.-H. Hsu, S. Raina, M. Howell, W. P. Kang and J.-H. Huang, *J. Renewable Sustainable Energy*, 2018, **10**, 063501.
42 G. Yue, R. Cheng, X. Gao, L. Fan, Y. Mao, Y. Gao and F. Tan, *Nanoscale Res. Lett.*, 2020, **15**, 179.
43 G. Wang, S. Kuang and W. Zhang, *Mater. Lett.*, 2016, **174**, 14–16.
44 L. Li, X. Zhang, Z. Li, S. Liu, X. Li, Y. Zhang and W. Zhang, *Mater. Today Commun.*, 2019, **18**, 1–6.
45 P. Joshi, L. Zhang, Q. Chen, D. Galipeau, H. Fong and Q. Qiao, *ACS Appl. Mater. Interfaces*, 2010, **2**, 3572–3577.
46 G. Veerappan, W. Kwon and S.-W. Rhee, *J. Power Sources*, 2011, **196**, 10798–10805.
47 Y. Zhu, S. Murali, W. Cai, X. Li, J. W. Suk, J. R. Potts and R. S. Ruoff, *Adv. Mater.*, 2010, **22**, 3906–3924.
48 X. Huang, X. Qi, F. Boey and H. Zhang, *Chem. Soc. Rev.*, 2012, **41**, 666–686.
49 C. Cui, W. Qian, Y. Yu, C. Kong, B. Yu, L. Xiang and F. Wei, *J. Am. Chem. Soc.*, 2014, **136**, 2256–2259.
50 W.-T. Wu, S.-H. Yang, C.-M. Hsu and W.-T. Wu, *Diamond Relat. Mater.*, 2016, **65**, 91–95.
51 F. Yu, Y. Shi, W. Yao, S. Han and J. Ma, *J. Power Sources*, 2019, **412**, 366–373.
52 B. Tang, H. Yu, W. Huang, Y. Sun, X. Li, S. Li and T. Ma, *RSC Adv.*, 2019, **9**, 15678–15685.
53 Y. Chen, Z. Jing and J. Miao, *J. Electroanal. Chem.*, 2020, **873**, 114344.

54 J. Y. Lee, G. H. Choi, J. Moon, W. S. Chi and J. T. Park, *Appl. Surf. Sci.*, 2021, **535**, 147637.
55 C. K. Kim, J.-M. Ji, H. Zhou, C. Lu and H. K. Kim, *Nanomaterials*, 2019, **10**, 29.
56 M. Younas, T. N. Baroud, M. A. Gondal, M. A. Dastageer and E. P. Giannelis, *J. Power Sources*, 2020, **468**, 228359.
57 G. Wang, L. Wang, W. Xing and S. Zhuo, *Mater. Chem. Phys.*, 2010, **123**, 690–694.
58 I. Juhász Junger, D. Wehlage, R. Böttjer, T. Grothe, L. Juhász, C. Grassmann, T. Blachowicz and A. Ehrmann, *Materials*, 2018, **11**, 1604.
59 W. Wei, H. Wang and Y. H. Hu, *Int. J. Energy Res.*, 2014, **38**, 1099–1111.
60 P. Jha, P. Veerender, S. P. Koiry, C. Sridevi, A. K. Chauhan, K. P. Muthe and S. C. Gadkari, *Polym. Adv. Technol.*, 2018, **29**, 401–406.
61 G. Wang, W. Dong, C. Yan, S. Hou and W. Zhang, *Mater. Lett.*, 2018, **214**, 158–161.
62 W. Hou, Y. Xiao, G. Han and H. Zhou, *Electrochim. Acta*, 2016, **190**, 720–728.
63 H. Li, Y. Xiao, G. Han and M. Li, *J. Mater. Sci.*, 2017, **52**, 8421–8431.
64 M. Kuo, T.-C. Cheng, H.-K. Ye, T.-L. Wang, T.-H. Wu, C.-C. Kuo and R.-H. Lee, *Catalysts*, 2021, **11**, 507.
65 L. Hou, W. Zhang, H. Zhou and H.-J. Zhai, *J. Nanopart. Res.*, 2020, **22**, 6.
66 M. U. Shahid, N. M. Mohamed, A. S. Muhsan, R. Bashiri, A. E. Shamsudin and S. N. A. Zaine, *Diamond Relat. Mater.*, 2019, **94**, 242–251.
67 J. Gao, Y. Yang, Z. Zhang, J. Yan, Z. Lin and X. Guo, *Nano Energy*, 2016, **26**, 123–130.
68 A. Zatirostami, *Thin Solid Films*, 2020, **701**, 137926.
69 K.-M. Lee, W.-H. Chiu, H.-Y. Wei, C.-W. Hu, V. Suryanarayanan, W.-F. Hsieh and K.-C. Ho, *Thin Solid Films*, 2010, **518**, 1716–1721.
70 P. Gemeiner, J. Kuliček, T. Syrový, A. Ház, V. Khunová, M. Hatala, M. Mikula, M. Hvojnik, L. Gál, M. Jablonský and M. Omastová, *Synth. Met.*, 2019, **256**, 116148.
71 J. Ma, S. Qingfeng, Z. Fengbao and W. Mingxing, *Mater. Res. Bull.*, 2018, **100**, 213–219.
72 Y.-M. Xiao, J.-Y. Lin, J.-H. Wu, S.-Y. Tai and G.-T. Yue, *Electrochim. Acta*, 2012, **83**, 221–226.
73 J. Song, G. R. Li, C. Y. Wu and X. P. Gao, *J. Power Sources*, 2014, **266**, 464–470.
74 Z. Jin, M. Zhang, M. Wang, C. Feng and Z.-S. Wang, *Acc. Chem. Res.*, 2017, **50**, 895–904.
75 C. Gao, Q. Han and M. Wu, *J. Energy Chem.*, 2018, **27**, 703–712.
76 A.-R. Ko, J.-K. Oh, Y.-W. Lee, S.-B. Han and K.-W. Park, *Mater. Lett.*, 2011, **65**, 2220–2223.
77 J. Kim, J. S. Kang, J. Jeong, Y. J. Son, M. J. Lee, J. Kang, A. Lim, H. S. Park and Y.-E. Sung, *J. Power Sources*, 2018, **396**, 213–219.
78 X. Yu, J. Zhu, F. Liu, J. Wei, L. Hu and S. Dai, *Sci. China: Chem.*, 2013, **56**, 977–981.
79 V. Subbiah, G. Landi, J. J. Wu and S. Anandan, *Phys. Chem. Chem. Phys.*, 2019, **21**, 25474–25483.
80 X. Zhang, J. Bai, M. Zhen and L. Liu, *RSC Adv.*, 2016, **6**, 89614–89620.
81 G. Wang, S. Hou, C. Yan, Y. Lin and S. Liu, *Chem. Eng. J.*, 2017, **322**, 611–617.
82 A. S. A. Ahmed, W. Xiang, A. Gu, X. Hu, I. A. Saana and X. Zhao, *New J. Chem.*, 2018, **42**, 11715–11723.
83 M. Wu, X. Lin, A. Hagfeldt and T. Ma, *Chem. Commun.*, 2011, **47**, 4535.
84 A. T. Yadav, P. P. Magar, V. S. Kadam, C. V. Jagtap and C. S. Pawar, *J. Mater. Sci.: Mater. Electron.*, 2016, **27**, 12297–12301.
85 C.-H. Tsai, P.-H. Fei, C.-M. Lin and S.-L. Shiu, *Coatings*, 2018, **8**, 21.